

Security Classification

DOCUMENT CONTROL DATA - R & D

(Security classification of title, body of abstract and indexing annotation must be entered when the overall report is classified)

1. ORIGINATING ACTIVITY (Corporate author) Naval Research Laboratory Washington, D.C. 20375		2a. REPORT SECURITY CLASSIFICATION Unclassified
2b. GROUP		
3. REPORT TITLE SOLAR IONIZATION RATES FOR THE IONOSPHERIC E, F, AND D REGIONS		
4. DESCRIPTIVE NOTES (Type of report and inclusive dates) This is an interim report on a continuing NRL problem.		
5. AUTHOR(S) (First name, middle initial, last name) A.W. Ali and P.C. Kepple		
6. REPORT DATE October 25, 1973	7a. TOTAL NO. OF PAGES 34	7b. NO. OF REFS 34
8a. CONTRACT OR GRANT NO. NRL Problem A03-19	9a. ORIGINATOR'S REPORT NUMBER(S) NRL Report 7598	
b. PROJECT NO. RR 011-09-01	9b. OTHER REPORT NO(S) (Any other numbers that may be assigned this report)	
c.		
d.		
10. DISTRIBUTION STATEMENT Approved for public release; distribution unlimited.		
11. SUPPLEMENTARY NOTES		12. SPONSORING MILITARY ACTIVITY Defense Advanced Research Projects Agency Arlington, Va. 22209 Office of Naval Research, Department of the Navy Arlington, Va. 22217
13. ABSTRACT		

Two approaches were taken to calculate the photoionization rates for the ionosphere. First, a detailed line-by-line deposition for the range 1-1215A was carried out by using experimental or theoretical absorption and ionization cross sections for the atmospheric species. The second approach was to contract these lines into bands having approximately 11 bands for each region, and to calculate the photoionization rate for these new bands. The total photoionization rates for the two methods agree very well.

Security Classification

14. KEY WORDS	LINK A		LINK B		LINK C	
	ROLE	WT	ROLE	WT	ROLE	WT
Solar flux Photoionization rates Photoabsorption cross sections Photoionization cross sections						

DD FORM 1 NOV 65 1473 (BACK)

(PAGE 2)

32

Security Classification

CONTENTS

Abstract	ii
Problem Status.....	ii
Authorization.....	ii
INTRODUCTION	1
SOLAR ULTRAVIOLET AND X-RAY FLUXES	2
ABSORPTION AND IONIZATION CROSS SECTIONS	2
Oxygen Atom.....	3
Molecular Oxygen	3
Molecular Nitrogen.....	4
Nitric Oxide	4
ION PRODUCTION RATES FROM ALL SOLAR LINES.....	5
ION PRODUCTION RATES BY REGROUPING SOLAR LINES	15
ACKNOWLEDGMENT	16
REFERENCES.....	17

ABSTRACT

Two approaches were taken to calculate the photoionization rates for the ionosphere. First, a detailed line-by-line deposition for the range 1-1215A was carried out by using experimental or theoretical absorption and ionization cross sections for the atmospheric species. The second approach was to contract these lines into bands having approximately 11 bands for each region, and to calculate the photoionization rate for these new bands. The total photoionization rates for the two methods agree very well.

PROBLEM STATUS

This is an interim report on one phase of a continuing NRL problem.

AUTHORIZATION

NRL Problem A03-19
Project RR 011-09-01

Manuscript submitted April 24, 1973.

SOLAR IONIZATION RATES FOR THE IONOSPHERIC E, F, AND D REGIONS

INTRODUCTION

In this report, the photoionization rates in the altitude region 80-500 km are calculated on the basis of the available data. To calculate these rates one needs the solar flux at the top of the atmosphere (550 km), the absorption and ionization cross sections of the atmospheric species over the entire range of the incident spectrum, and the densities of these species.

Let $R_j(h)$ indicate the photoionization rate ($\text{cm}^{-3}\text{s}^{-1}$) of species j whose density is $N_j(h)$ at an altitude h . Let $\sigma_n(j,\lambda)\dagger$ denote the absorption or the ionization cross sections for species j at wavelength λ . Then the ion production rate from species j for an overhead sun is*

$$R_j(h) = \sum_{\lambda} \Phi_0(\lambda) \sigma_i(j,\lambda) N_j \exp \left[- \sum_{j,\lambda} \int_h^{\infty} \sigma_T(j,\lambda) N_j(h) dh \right], \quad (1)$$

where $\Phi_0(\lambda)$ is the flux (in photons/cm²/s) for a given wavelength at the top of the atmosphere. The upper limit here represents 550 km.

The solar flux data used in this report are taken from the latest values as given by Hinteregger (1) for the spectral range 1310-33.6 Å. These data are for a nonflaring sun with medium activity corresponding to a flux of $130-170 \times 10^{-22} \text{ W/m}^2/\text{Hz}$ for the solar radio noise at 10.7 cm. The x-ray data in the range 10-1 Å are from Swider (2) for a non-flaring, quiet sun. The densities of the major species above 120 km are from a model atmosphere by Jacchia (3). For altitudes below 120 km, CIRA (4) is used. The absorption and the ionization cross sections are from various experimental and theoretical sources, and thus are referenced in the third section.

The deposition of the radiation from the sun into the upper atmosphere plays an important, if not the dominant, role in heating the atmosphere. In this report we concern ourselves with the ion production rates in the F, E, and D regions of the ionosphere as the result of the deposition of the ultraviolet (UV) and x-ray radiation (1310-1 Å). This calculation, therefore, will also be helpful in the calculations of the electron temperature in the ionosphere. Such a calculation has been done by Dalgarno et al. (5) for the F and E regions of the ionosphere using the incident solar fluxes from Watanabe and Hinteregger (6), who have calculated the photoionization rates for the E and F regions. Nicolet and Aikin (7) have discussed the formation of the D region of the ionosphere and indicated that Lyman α and the soft x rays are responsible for the ionization of the D region in addition to the cosmic rays.

*For other Zenith angles one must integrate along the actual path of a ray.

$\dagger n = T$ for absorption, $n = i$ for ionization.

The initial ion production rates were calculated using the individual lines and continuum bands as given by Hinteregger (1). However, an attempt was also made to reduce these lines by regrouping them with average cross sections and the appropriate flux values. This is discussed in the fifth section.

In addition to the ion formation rates, the transmittances

$$\exp \left[- \sum_j \int \sigma_T (j, \lambda) N_j(h) dh \right]$$

of the strongest lines were also calculated to show their penetrability from the top of the atmosphere downwards.

SOLAR ULTRAVIOLET AND X-RAY FLUXES

In Table 1 we present the solar flux values in the range 1310-1Å. Here, the latest flux values for the solar lines and the continuum emissions in the range 1310-33.6Å are from Hinteregger (1). These results are for a nonflaring (quiet) sun with medium activity corresponding to a flux of $130-170 \times 10^{-22} \text{ W/m}^2/\text{Hz}$ for the solar radio noise at 10.7 cm. The data from 10-1Å are from Swider (2) for a quiet sun.

The ion production rate from a given species (see Eq. (1)) is proportional to the ionization cross section, the flux values at the top of the atmosphere, and the number density of the species. Thus an uncertainty by a factor of 3 (for example) in the flux value would make the ion production rate uncertain by the same factor. Therefore, more reliable measurements of the UV, extreme UV, and x rays should be made. It is of utmost importance, especially for the ionospheric modeling, to have a measuring device such as a satellite relaying these fluxes continuously to the ground monitoring stations. An ionospheric model, to predict the diurnal, seasonal, and flare conditions, must have the instantaneous values of the solar fluxes. Solrad (8,9) satellites could and should serve as potential solar flux measurement devices. Table 2, (10) for example, gives the sensors aboard NRL/NASA Solrad 10 that measure UV and x rays from 1700-0.1Å solar radiation. However, in future Solrads, it would be desirable to have the spectral range in the 1350-30Å region further divided into smaller bands. We will come to this point later.

ABSORPTION AND IONIZATION CROSS SECTIONS

The dominant atmospheric species in the region of interest for this report are O, N₂, and O₂. However, since the major ionization source (7) in the D region is NO, Table 3 gives the cross-sectional data for NO in addition to those for the major atmospheric species. Effective ionization cross sections are given whenever the ejected photoelectron's energy exceeds 30 eV.

Oxygen Atom

The oxygen atom is an important ionization source in the upper atmosphere. In fact, it is the major source above 250 km. Oxygen has several ionization continua that have to be considered for two important reasons:

1. To calculate accurately! the ejected photoelectron's energies.
2. To determine the percentage of the metastable $O^+(^2D)$ thus created.

This metastable ion charge exchanges rapidly (11) with N_2 ($k \approx 1 \times 10^{-9}$) (Ref. 12) whose ion disappears quickly via dissociative recombination with free electrons ($k \approx 2 \times 10^{-7} \text{ cm}^3/\text{s}$ at 300°K) (Ref. 13). Dalgarno et al. (14) have calculated the photoionization cross section of oxygen atom, giving the partial cross sections for the following ionization continua: $O^+(1S^2 2S^2 2P^3) ^4S, ^2D, ^2P$ and $O^+(1S^2 2S 2P^4) ^4P, ^2P$. In addition to the ground ionic state 4S , which is populated from 4P state, we need only consider $O^+(^2D)$ which in turn is populated by 2P states. In this approach we follow Dalgarno and McElroy (15); however, we shall utilize the partial photoionization cross sections for $^4S, ^2D$, and 2P of Henry (16) which is a close coupling calculation. These cross sections are shown on Fig. 1. For the inner-shell photoionization cross sections we utilize calculations of Dalgarno et al. (14). The effective ionization cross sections resulting in $O^+(^4S)$ and $O^+(^2D)$ are given in Table 3. However, the experimental cross section of Cairns and Samson (17) is higher than the calculated one, from the first ionization threshold down to 600\AA , below which the agreement is reasonable. In the $900\text{-}800\text{\AA}$ region the experimental value is 5-6 Mb compared to the calculated 3-3.2 Mb. Between 800\AA and 600\AA the disagreement is better than a factor of 2. Therefore, we multiplied Henry's results by approximately 1.5. For wavelengths shorter than 100\AA , the ionization cross sections given in Table 3 are derived from the x-ray mass absorption results, which are discussed below.

Molecular Oxygen

The absorption cross sections for molecular oxygen have been measured below 1300\AA by Watanabe (18), Cook and Metzger (19), Matsunaga and Watanabe (20), Samson and Cairns (21-22), and Huffman et al. (23). For a detailed comparison of these experimental values see the review article by Hudson (24). Where one measurement is favored over another, the values quoted in Table 3 are indicated by an appropriate reference. Where more than one measurement exists, the discrepancies between the cross sections are within 20% except in the range $700\text{-}600\text{\AA}$ where a discrepancy of about 80% is obvious. Data in the $600\text{-}200\text{\AA}$ range are exclusively from Ref. 22. From 200\AA to 100\AA Henry's theoretical values for oxygen atom (16) are multiplied by 2. Below 100\AA Victoreen's empirical formulas for N and O in the range $\lambda \leq 30\text{\AA}$ (25) and Messner's data (2) for wavelengths between 30 and 100\AA were utilized, and the results for absorption cross sections are given in Table 3.

Molecular oxygen has several ionization continua, and one must consider these in order to calculate the ejected photoelectron's energies. However, partial photoionization cross sections for O_2 are available (26) only in the range of $600\text{-}700\text{\AA}$, which is a very limited range.

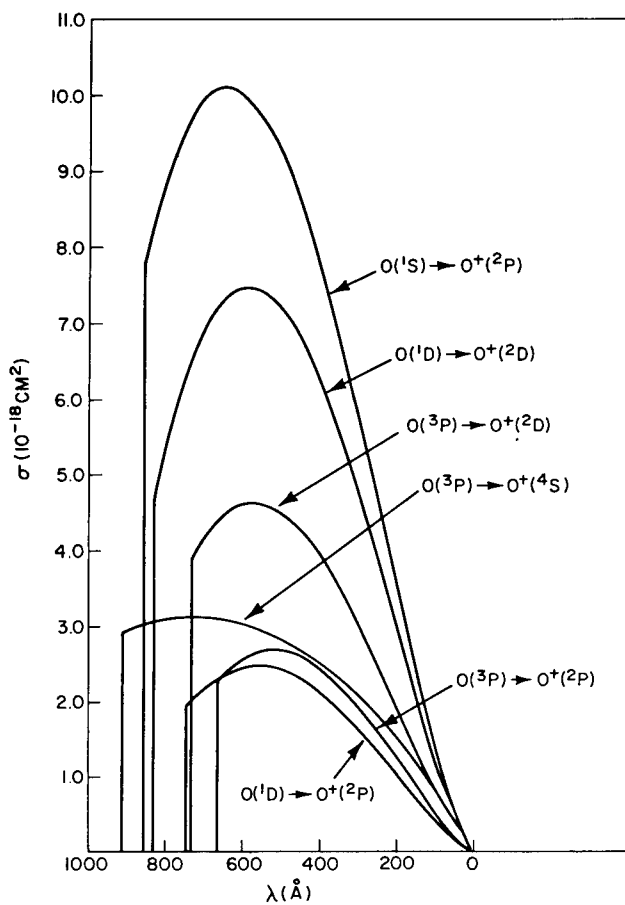


Fig. 1 — Oxygen partial photoionization cross sections as a function of wavelength

Molecular Nitrogen

The photoionization and the photoabsorption cross sections for N_2 have been measured by Huffman et al. (27), Cook and Metzger (19), Samson and Cairns (21,22), and by Watanabe and Marmo (28). For the range of 1-100 Å we have used the cross section mentioned in the previous section; for 100-200 Å we used Henry's (16) calculations (which are shown in Fig. 2) multiplied by 2. For the range 200-600 Å we have relied mainly on the data in Refs. 21 and 22. In the remaining 600-1300 Å range we have indicated the references from which the data are taken. These are all given in Table 3. Partial photoionization cross sections for different ionization continua of N_2 have been measured by Blake and Carver (29), but for a limited range only.

Nitric Oxide

The absorption and the ionization cross sections of NO between 1300 and 600 Å used in this report are due to Watanabe et al. (30). Below this range, down to 1 Å, the absorption and the ionization cross sections for NO were obtained from the sum of the corresponding values of N_2 and O_2 divided by 2.

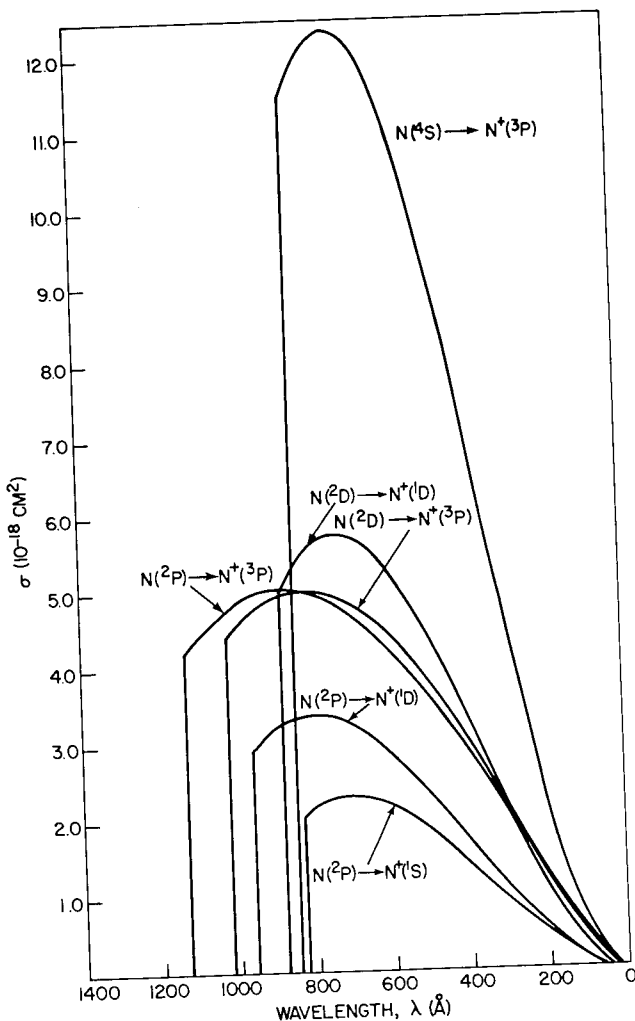


Fig. 2 — Nitrogen partial photoionization cross sections as a function of wavelength

ION PRODUCTION RATES FROM ALL SOLAR LINES

Using the values of the solar fluxes given in Table 1 and the corresponding absorption and ionization cross sections given in Table 3, we have calculated the ion production rates. Table 4 shows the ion production rates per species (O , O_2 , N_2) as a function of altitude (80-500 km). These rates were obtained by summing the ion production rate from each of 83 lines. This table also gives the total electron production rate from O , O_2 , and N_2 . These results are shown in Fig. 3. On the other hand, the ion production rate from NO due to Lyman α alone is shown in Fig. 4.

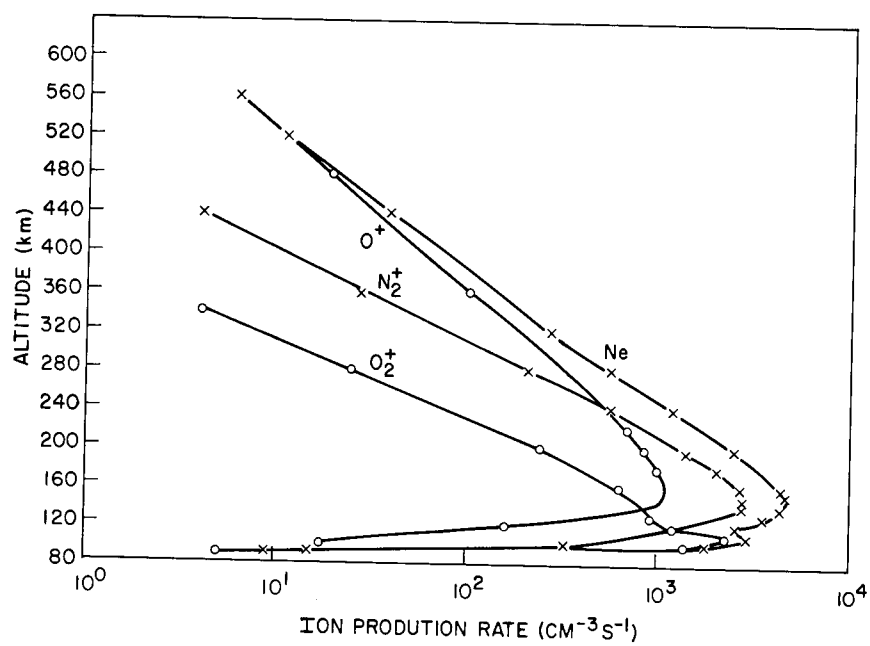


Fig. 3 — Total electron production rate profile

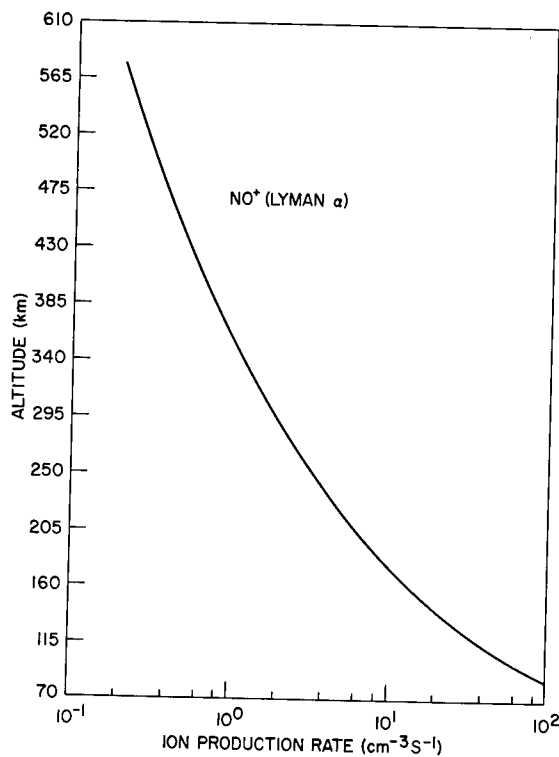


Fig. 4 — Production rate of NO^+ from Lyman α as a function of altitude

Figures 5-11 show the ion production rates of some important lines or bands which ionize one or all of the dominant atmospheric species. Figure 5, for example, shows the ion production rates from O_2 due to 1025.7, 990, and 977 Å. The peak production rates due to these lines occur in the altitude region of 100-120 km where a comparison of Fig. 5 and Table 4 shows that these lines are the dominant sources of O_2^+ which in turn comprises approximately 50% of the total ion production rate. Other important lines or bands are as follows:

- 370-270 Å, which produces 15% of the total ions from N_2 at 160 km
- 303.8 Å, which produces 25% of the total ions from N_2 at the same altitude
- 280-231 Å, which produces about 12% of N_2^+ at 145 km
- 176-153 Å, which produces approximately 7% of N_2^+ at 130 km

The production rates of these lines or bands are shown in Figs. 5-11. Therefore, it seems appropriate to emphasize these lines in future Solrad UV and x-ray measuring devices.

The transmittances of the above lines and bands are shown in Figs. 12 and 13 to indicate their penetrability from the top of the atmosphere downward.

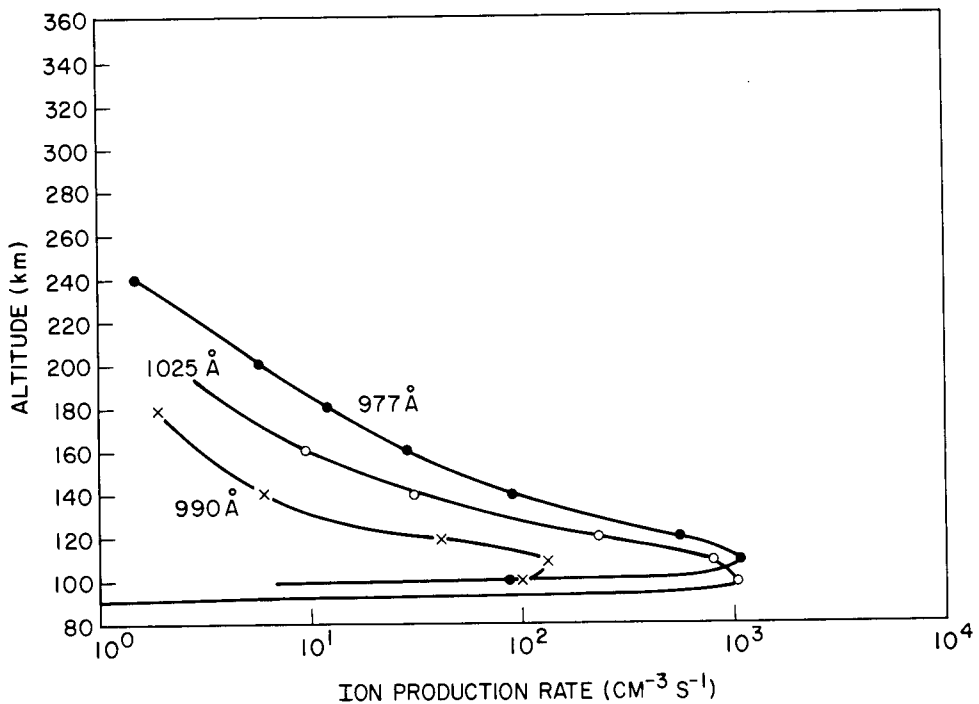


Fig. 5 — Ion production rates from O_2 for solar lines 1025, 990, and 977 Å

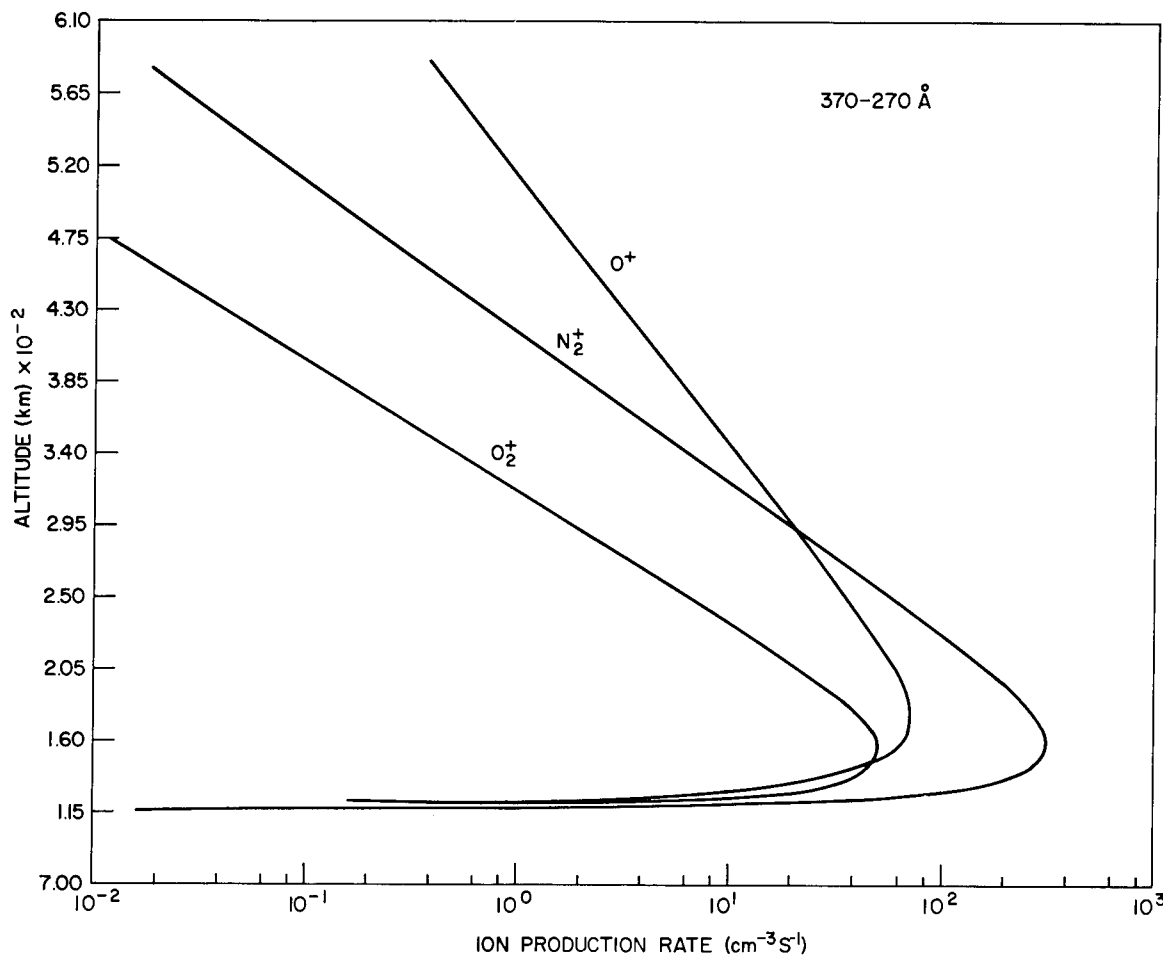


Fig. 6 — Ion production rate profiles for the band 370 to 360Å

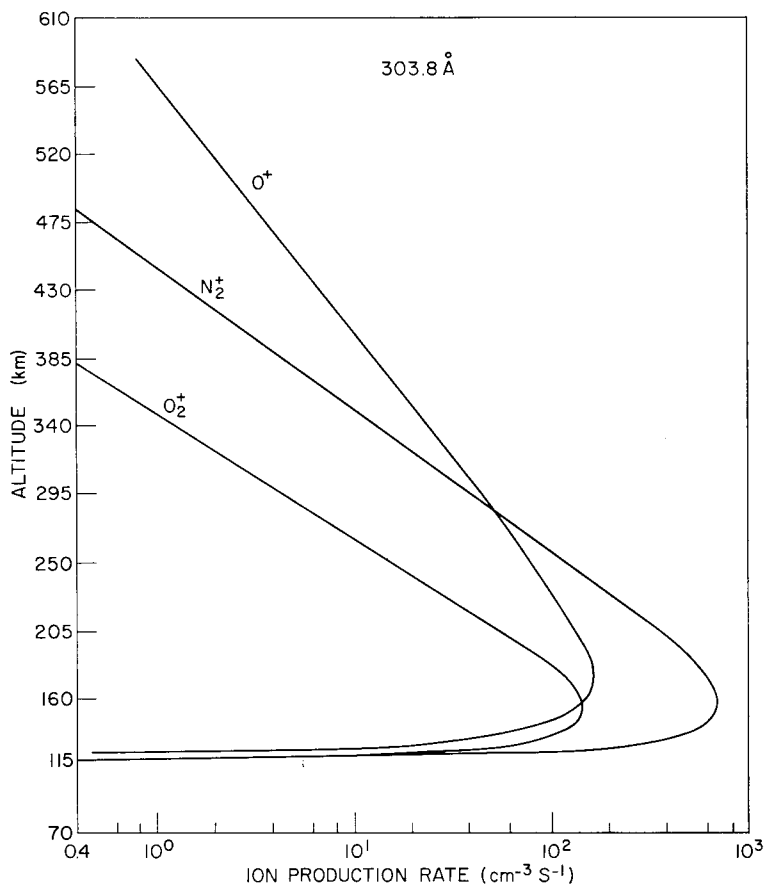


Fig. 7 — Ion production rate profiles for 303.8Å

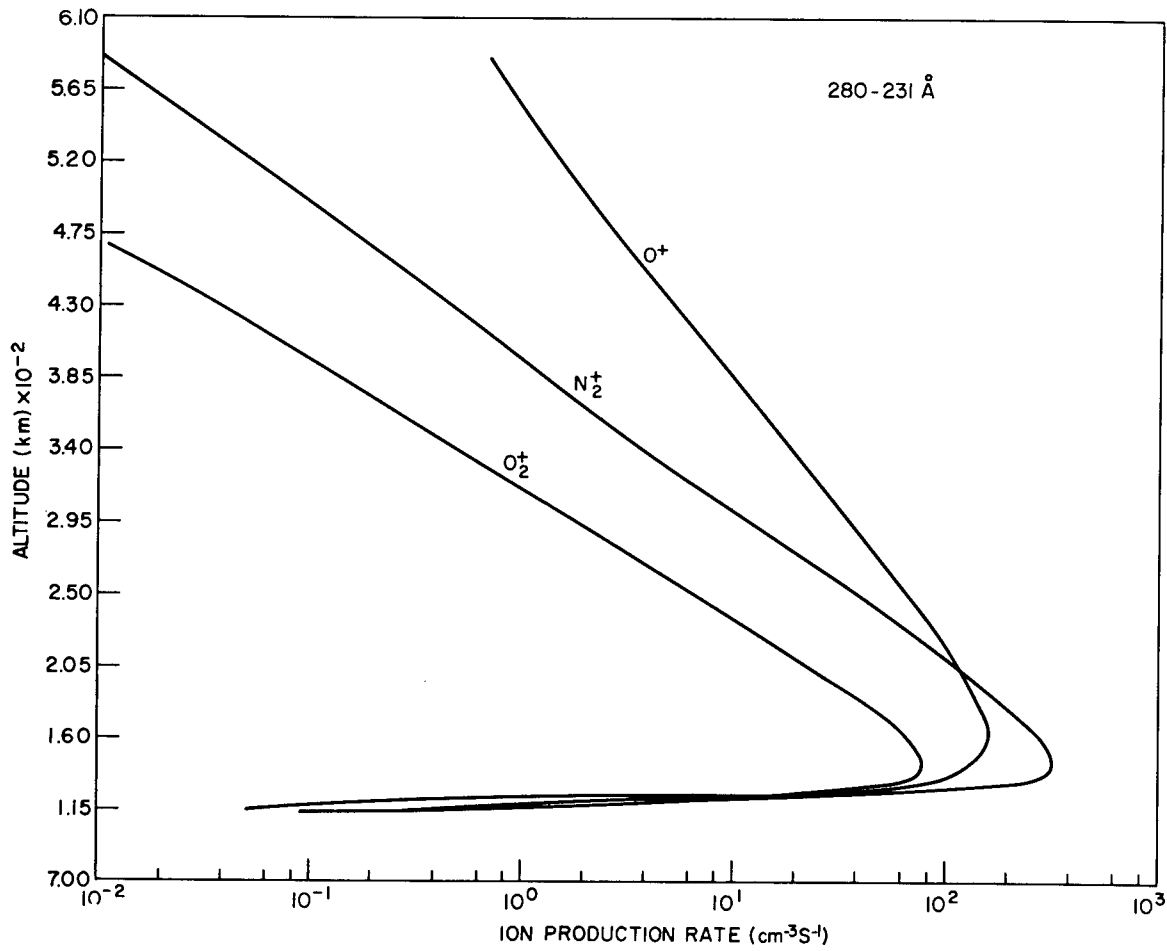


Fig. 8 — Ion production rate profiles for the band 280 to 231 Å

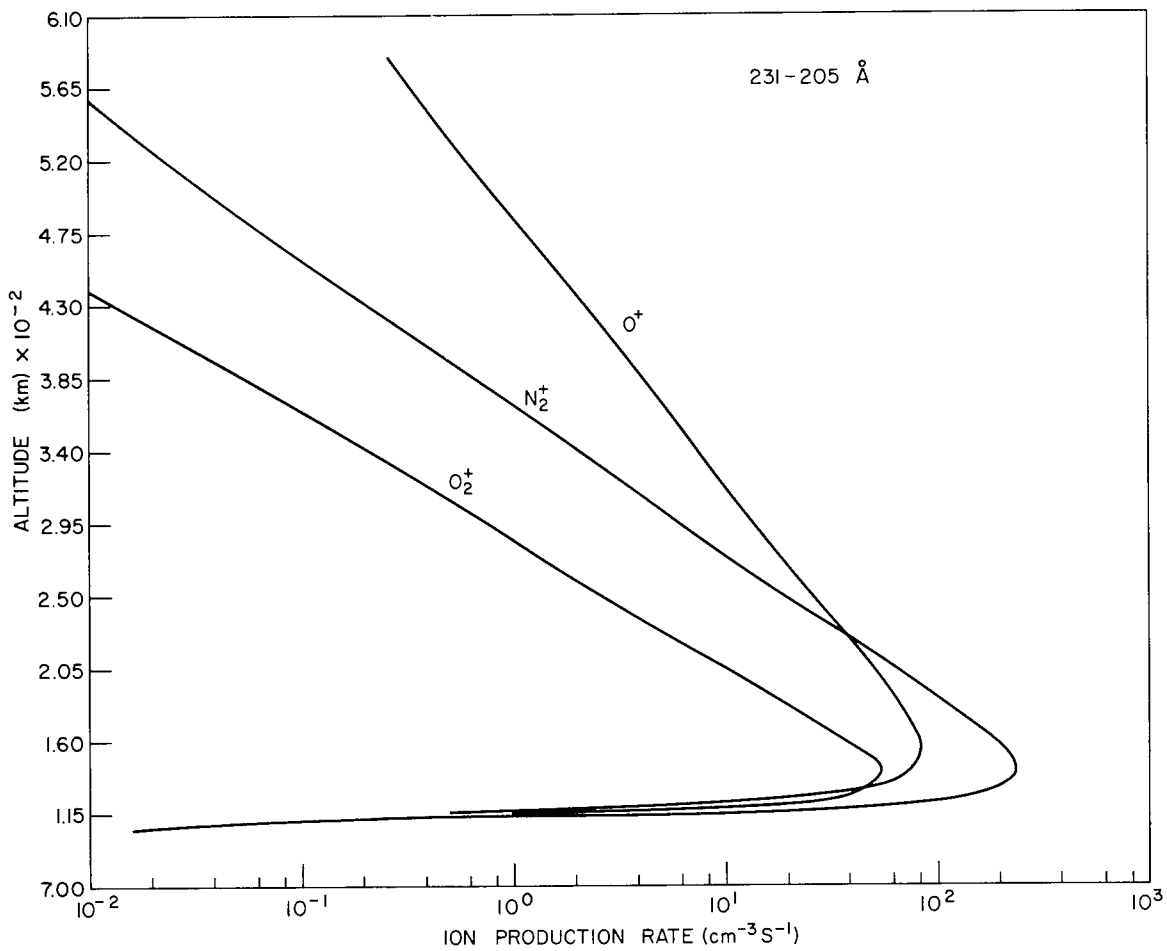


Fig. 9 — Ion production rate profiles for the band 231 to 205 Å

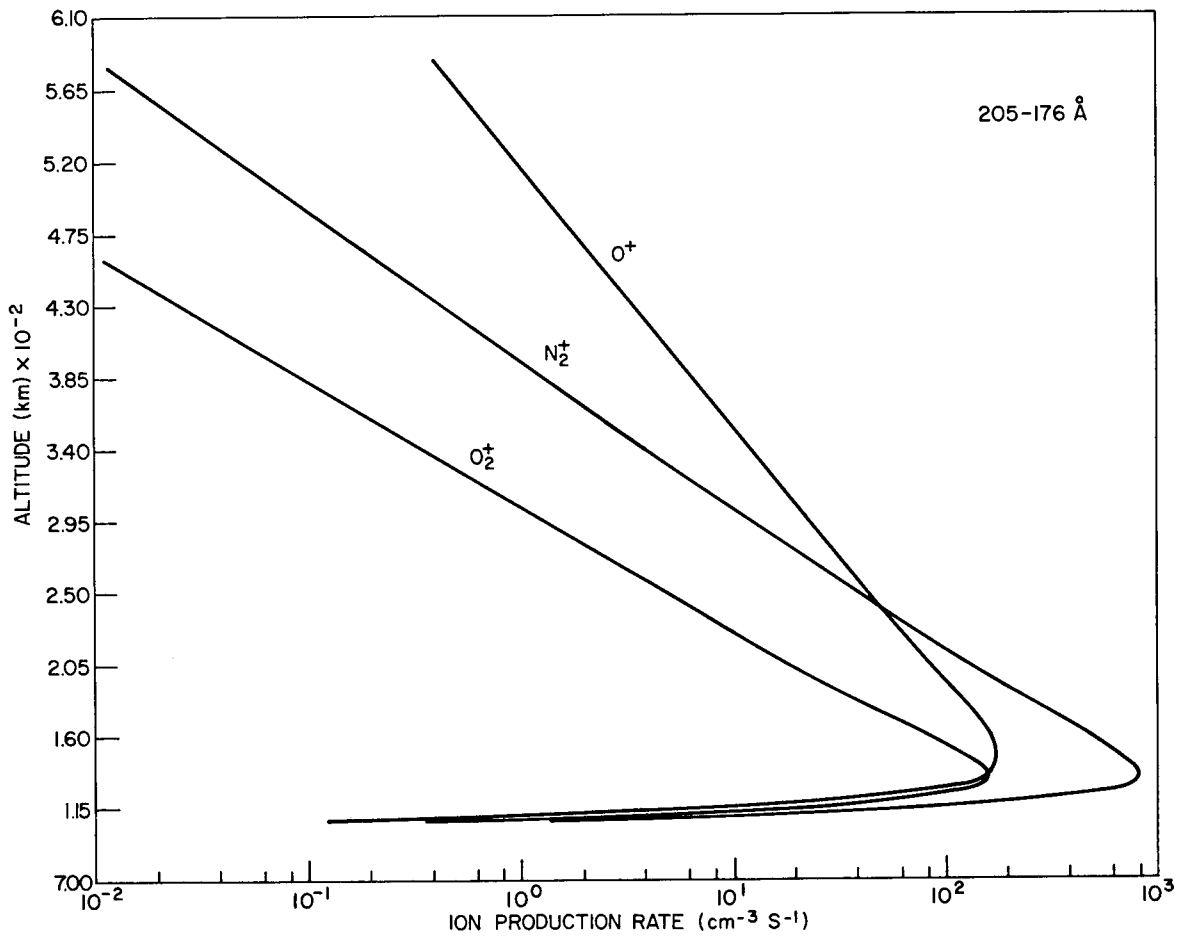


Fig. 10 — Ion production rate profiles for the band 205 to 176 Å

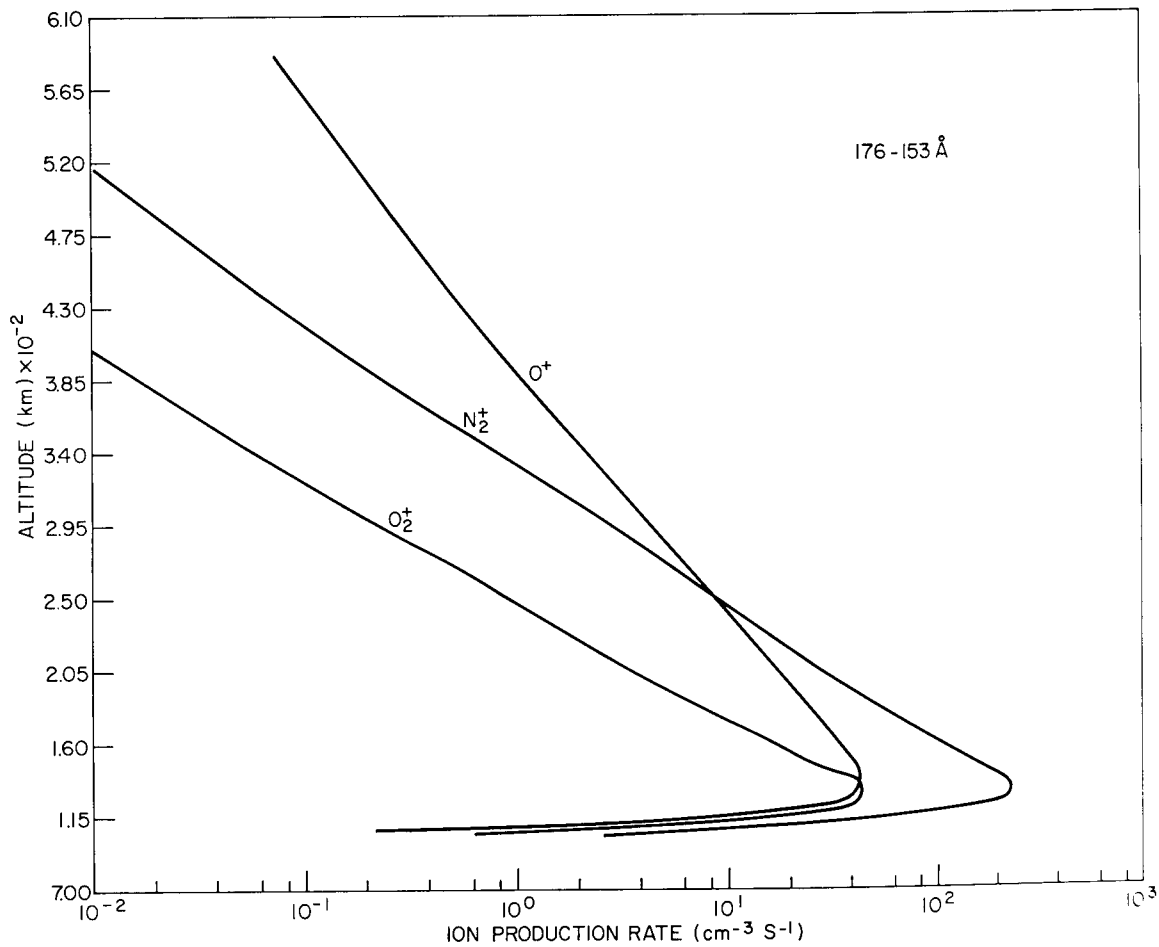


Fig. 11 — Ion production rate profiles for the band 176 to 153Å

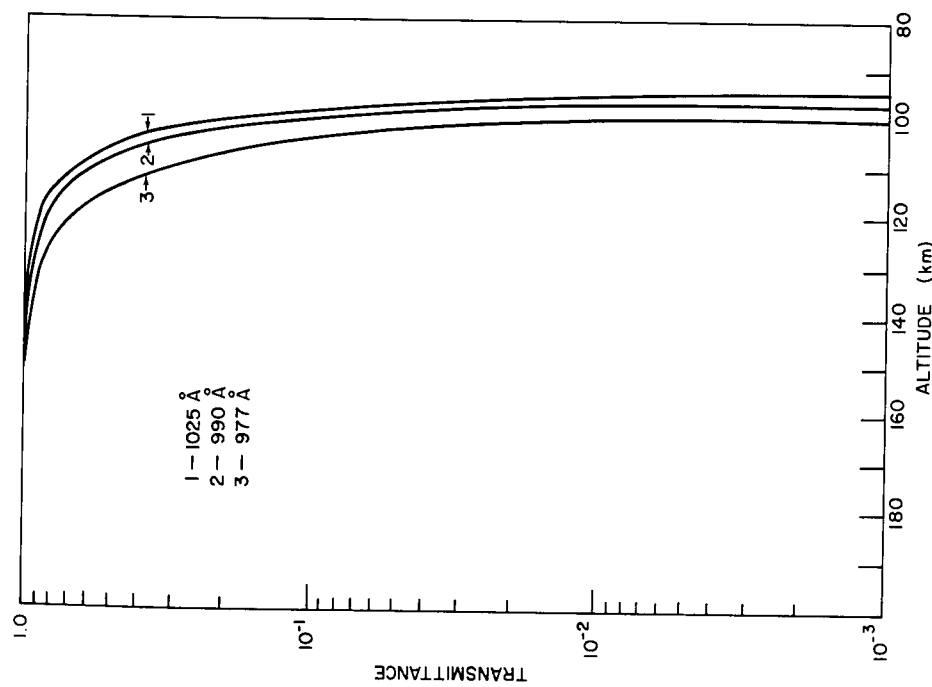


Fig. 12 — Transmittances of solar lines 1025, 990,
and 977 Å as a function of altitude

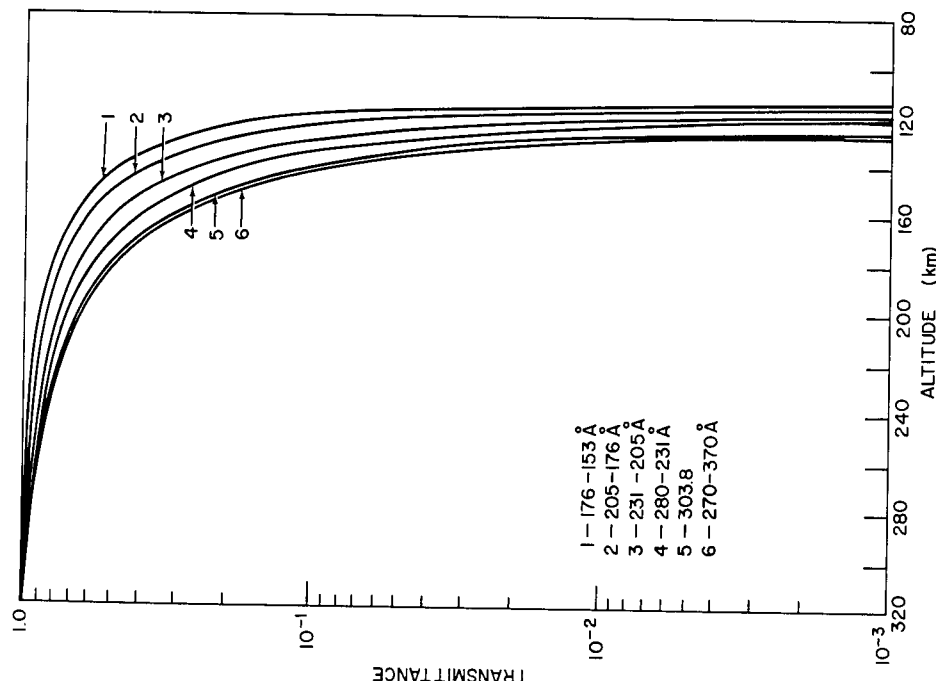


Fig. 13 — Transmittances of six solar bands
as a function of altitude

ION PRODUCTION RATES BY REGROUPING SOLAR LINES

To reduce the amount of computation, the lines and bands given in the second section are grouped into 22 bands. In performing this grouping we demand that the ion production rates remain unchanged to within a few percent. We recall that these rates, as expressed in Eq. (1), can be rewritten as

$$R_j(h) = N_j(h) \sum_{\beta} \sum_{\lambda \in \beta} \sigma_i(j, \lambda) \Phi_0(\lambda) \times \exp \left[- \int_h^{\infty} \sum_i N_i(h) dh \sigma_T(i, \lambda) \right], \quad (2)$$

where the sums are over the new bands β and the individual lines which comprise the bands.

We need to find average cross sections such that

$$R_j(h) = N_j(h) \sum_{\beta} \sigma_i(j, \beta) \Phi_0(\beta) \exp \left[- \int_h^{\infty} \sum_i N_i(h) dh \sigma_T(i, \beta) \right], \quad (3)$$

where $\Phi_0(\beta) = \sum_{\lambda \in \beta} \Phi_0(\lambda)$. Thus

$$\sigma_i(j, \beta) = \frac{\sum_{\lambda \in \beta} \sigma_i(j, \lambda) \Phi_0(\lambda) \exp \left[- \sum_i \int_h^{\infty} N_i(h) dh \sigma_T(i, \lambda) \right]}{\sum_{\lambda \in \beta} \Phi_0(\lambda) \exp \left[- \sum_i \int_h^{\infty} N_i(h) dh \sigma_T(i, \beta) \right]}. \quad (4)$$

If one can assign an average σ_T to the band, then the exponential in the numerator can be removed from the summation and canceled along with the one in the denominator. This leads to

$$\sigma_i(j, \beta) = \frac{\sum_{\lambda \in \beta} \sigma_i(j, \lambda) \Phi_0(\lambda)}{\sum_{\lambda \in \beta} \Phi_0(\lambda)}, \quad (5)$$

or, the ionization cross section for the band is the average of the cross sections of the lines in the band, weighted by the fluxes. This is not at all surprising, but it is important to note that the correctness of this statement is limited by the correctness of the assignment of $\sigma_T(i, \beta)$ for all species O, N₂, and O₂.

The final partition into bands and the corresponding cross sections were arrived at after some trial and error. The new bands, along with a listing of the old lines and bands which they comprise, are shown in Table 5. It was found to be best to assign to σ_T an average weighted by the fluxes, just as for σ_i . The fluxes and cross sections appropriate to the new bands are shown in Table 6.

The ion production rates due to the new bands for (O , N_2 , O_2) and their sum as a function of altitude are given in Table 7. A comparison with Table 4 indicates excellent agreement between the two approaches.

Finally, Table 8 gives the densities of the dominant atmospheric species of N_2 , O , and O_2 as calculated from Jacchia (3) and CIRA (4). For the minor species NO, Strobel's calculated values (31) are also given in Table 8.

Using Strobel's calculated NO values and the measured NO values of Barth (32), the NO^+ production rate for the D region is shown along with the other ion production rates (Figs. 14 and 15). One could also use the latest measured values of NO by Meira (33) to calculate the NO^+ production rate. However, it appears that the NO^+ production rate exceeds (34) the known rate of loss, adding to the many uncertainties in the D region.

ACKNOWLEDGMENT

We wish to thank Dr. E. Hyman of Science Application, Inc., Arlington, Va., for his help with the preparation of Table 3.

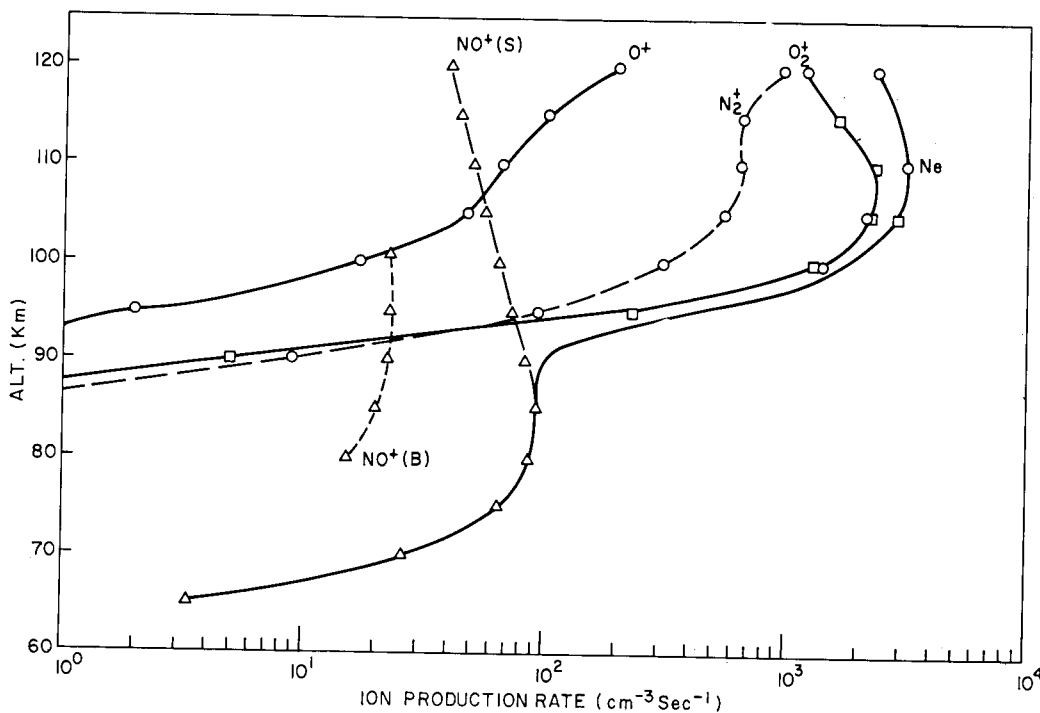


Fig. 14 — D-region total electron production profile

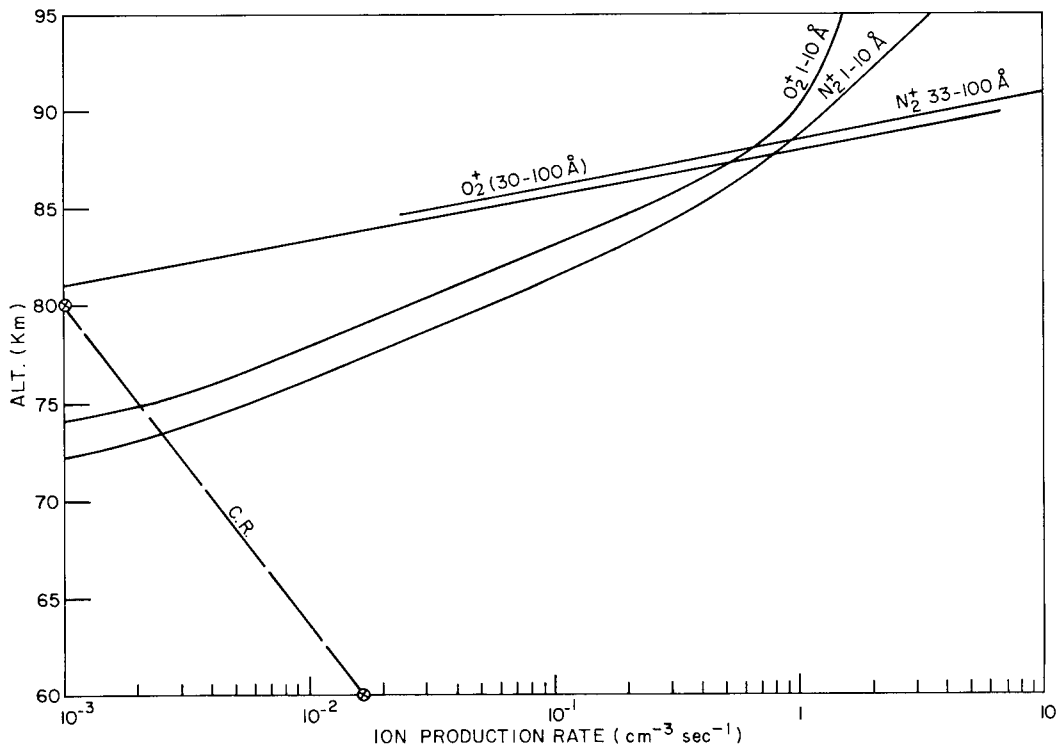


Fig. 15 — Ion production rates for the bands 1 to 10 Å and 33 to 100 Å

REFERENCES

1. H.E. Hinteregger, Ann de Géophys. **26**, 547 (1970).
2. W. Swider, Jr., Rev. of Geophys. **7**, 573 (1969).
3. L.G. Jacchia, "Smithsonian Institution Astrophysical and Observatory Report," Smithsonian Institute, Washington, D.C., 1965.
4. "CIRA 1965," North-Holland Publishing Co., Amsterdam, 1965.
5. A. Dalgarno, M.B. McElroy, and R.J. Moffett, Planet. Space Sci., **11**, 463 (1963).
6. K. Watanabe and H.E. Hinteregger, J. Geophys. Res. **67**, 999 (1962).
7. M. Nicolet and A.C. Aikin, J. Geophys. Res. **65**, 1469 (1960).
8. R.W. Kreplin and D.M. Horan, "The NRL Solrad 9 Satellite, Solar Explorer B, 1968-17 Å," NRL Report 6800 March 24, 1969.
9. D.M. Horan and R.W. Kreplin, "The Solrad 10 Satellite, Explorer 44, 1971-058 Å," NRL Report 7408, July 12, 1972.
10. R.W. Kreplin, private communication.
11. R.F. Stebbings, B.R. Turner, and J.A. Rutherford, J. Geophys. Res. **71**, 771 (1966).
12. F.R. Gilmore, E. Bauer, and J.W. McGowan, J. Quant. Spect. Rad. Transfer, **9**, 157 (1969).

13. F.J. Mehr and M.A. Biondi, Phys. Rev. **181**, 264 (1969).
14. A. Dalgarno, R.J.W. Henry, and A.L. Stewart, Planet. Space Sci. **12**, 235 (1964).
15. A. Dalgarno and M.B. McElroy, Planet. Space Sci., **13**, 947 (1965).
16. R.J.W. Henry, J. Astrophys. **161**, 1153 (1970).
17. R.B. Cairns and J.A.R. Samson, Phys. Rev. **139**, A1403 (1965).
18. K. Watanabe, Advan. Geophys. **2**, 153, (1958).
19. G.R. Cook and P.H. Metzger, J. Chem. Phys., **41**, 321 (1964).
20. F.M. Matsunaga and K. Watanabe, Sci. Light **16**, 31 (1967).
21. J.A.R. Samson and R.B. Cairns, J. Geophys. Res. **69**, 4583, (1964).
22. J.A.R. Samson and R.B. Cairns, J. Opt. Soc. Amer. **55**, 1035 (1965).
23. R.E. Huffman, J.C. Larrabee and Y. Tanaka, J. Chem. Phys. **40**, 356 (1964).
24. R.D. Hudson, Rev. Geophys. Space Phys., **9**, 305 (1971).
25. J.A. Victoreen, J. Appl. Phys., **20**, 1141 (1949).
26. A.J. Blake and J.H. Carver, Phys. Lett. **19**, 387 (1965).
27. R.E. Huffman, Y. Tanaka, and J.C. Larrabee, J. Chem. Phys. **39**, 910 (1963).
28. K. Watanabe and F.F. Marmo, J. Chem. Phys. **25**, 965 (1956).
29. A.J. Blake and J.H. Carver, J. Chem. Phys. **47**, 1038 (1967).
30. K. Watanabe, F.M. Matsunaga, and H. Sakai, Appl. Opt. **6**, 391 (1967).
31. D.F. Strobel, J. Geophys. Res. **76**, 2441 (1971).
32. C.A. Barth, Ann de. Géophys. **22**, 198 (1966).
33. L.G. Meira, Jr., J. Geophys. Res. **76**, 202 (1971).
34. C.F. Sechrist, Jr., J. Atm. Terr. Phys. **34**, 1565 (1972).

Table 1
Solar Flux Value for Each Line or Band Between 1310 and 1Å

Line Element No.	Wavelength (Å)	Photon Energy (eV)	Flux
82 O _I	1304.9	9.50	9.9(8)
81 O _I	1302.2	9.52	5.4(8)
80 Si _{II}	1265	9.80	4.6(8)
79 Si _{II}	1260.7	9.83	2.3(8)
78 N _V	1242.8	9.98	2.9(8)
77 N _V	1238.8	10.01	4.3(8)
69 H _I	1215.7	10.20	3.0(11)
76 Si _{III}	1206.5	10.28	3.6(9)
75 C _{III}	1175	10.55	2.2(9)
74 Si _{IV}	1128.3	10.99	2.7(8)
73 Si _{IV}	1122.5	11.04	2.2(8)
72 N _{II}	1085	11.43	5.9(8)
71 O _{VI} , C _{II}	1037.6	11.95	1.7(9)
70 O _{III}	1031.9	12.01	2.3(9)
	1310-1027		3.7(9)*
68 H _I	1025.7	12.09	3.5(9)
67 N _{III}	990.0	12.50	6.0(8)
66 C _{III}	977.0	12.69	4.4(9)
65 H _I	972.5	12.75	8.0(8)
64 H _I	949.7	13.05	3.9(8)
63 S _{VI}	944.5	13.13	1.0(8)
62 H _I	937.8	13.22	2.2(8)
61 S _{VI}	933.4	13.28	1.3(8)
60 H _I	930.7	13.32	1.3(8)
59 H _I	926.2	13.39	1.3(8)
58 Unres.	1027-911	12.07-13.6	1.21(9)
57 Cont.	911-890	13.61-13.93	3.2(9)
56 C _{II}	904	13.7	1.3(8)
55 H _{cont.}	890-860	13.9-14.42	2.7(9)
53 H _{cont.}	860-830	14.4-14.9	1.5(9)
52 O _{II}	835	14.85	5.2(8)
51 H _{cont.}	830-800	14.9-15.5	7.8(8)

*Individual lines within integral bands are not considered separately.

Table 1 (Continued)

Line Element No.	Wavelength (Å)	Photon Energy (eV)	Flux
54 Unres.	911-800	13.6-15.5	1.0(8)
50 H _{cont.}	800-770	15.5-16.1	3.9(8)
49 O _{IV}	790.1	15.69	2.6(8)
48 O _{IV}	787.7	15.74	1.3(8)
47 S _V	786.5	15.76	8.0(7)
46 Ne _{VIII}	780.3	15.89	1.2(8)
45 Ne _{VIII}	770.4	16.09	2.3(8)
43 H _{cont.}	770-740	16.1-16.5	1.9(8)
44 N _{IV}	765.1	16.20	1.8(8)
42 O _V	760.4	16.30	8.0(7)
41 H _{cont.}	740-710	16.75-17.4	9.0(7)
40 H _{cont.}	710-680	17.46-18.23	4.0(7)
39 O _{III}	703.0	17.60	2.3(8)
38 Unres.	800-630	15.5-19.7	3.9(8)
37 O _V	629.7	19.69	9.2(8)
36 Mg _X	625.3	19.83	2.5(8)
35 Mg _X	609.8	20.33	5.0(8)
34 O _{III}	599.6	20.68	8.0(7)
33 HeI	584.3	21.22	8.9(8)
32 O _{IV}	554	22.40	3.1(8)
31 Si _{XII}	521	23.80	1.9(8)
30 O _{III}	508	24.40	8.0(7)
28 HeI _{cont.}	504-425	24.6-29.2	5.0(8)
29 Si _{XII}	499.3	24.83	3.8(8)
28 Ne _{VII}	465.2	26.65	1.6(8)
27 Unres.	630-460	19.7-27.0	4.4(8)
26 Unres.	460-370	27.0-33.5	0.6(9)
25 Mg _{IX}	368.1	33.68	5.6(8)
24 Unres.	365	34.0	1.7(8)
23 Fe _{XVI}	360.7	34.37	3.6(8)
22 Fe _{XVI}	335.4	36.9	7.2(8)
21 He _{II}	303.8	40.81	5.4(9)
20 Fe _{XV}	284.1	43.64	1.1(9)

Table 1 (Continued)

Line Element No.	Wavelength (Å)	Photon Energy (eV)	Flux
19 Unres.	370-270	33.5-45.9	2.03(9)
18 Integral	280-231	44.3-53.6	3.1(9)
17 Integral	231-205	53.6-60.4	1.4(9)
16 Integral	205-176	60.4-70.0	3.7(9)
15 Integral	176-153	70.0-81.	9.0(8)
14 Integral	153-100	81-124.	4.0(8)
13 Fe _X	94.0-96.1	132-139	1.6(7)
	100-90	124-137.8	9.9(7)
12 Integral	80-90	154-142.8	1.2(8)
11 Fe _{XIII}	76.0	163.1	8.0(6)
	80-70	155-177.1	9.4(7)
10 Fe _{XVI}	66.3	187.	7.0(6)
	70-60	177.1-206.6	1.0(8)
9 Si _{X/IX}	50.5-50.7	245.5-224	2.4(7)
8 Si _{X/IX}	60-50	206.6-248.	8.3(7)
7 Si _{XII}	44.1	281	6.0(6)
	50-40	248-310	4.7(7)
6 C	33.6	369	4.0(6)
5	9.0	1377.5	1.8(5)
4	7.0	1771.	2.8(4)
3	5.0	2479.	2.5(3)
2	3.0	4133.	3.0
1	1.0	12398.	0.1

Table 2
NRL/NASA Solrad 10 (C) Experiments

No.	Parameter	Sensor	Purpose
1A	0.5 - 3 Å	Ionization Chamber	Solar X-ray Monitor
1B	0.5 - 3 Å	Parallel Plate Ionization Chamber	Solar X-ray Monitor
2	1 - 5 Å	Ionization Chamber	Solar Electron Temperature
3A	1 - 8 Å	Ionization Chamber	Solar X-ray Monitor
3B	1 - 8 Å (Back-up)	Ionization Chamber	Solar X-ray Monitor
4A	8 - 16 Å	Ionization Chamber	Solar X-ray Monitor
4B	8 - 16 Å (Back-up)	Ionization Chamber	Solar X-ray Monitor
5	1 - 20 Å,	Ionization Chamber	Solar X-ray Monitor
	44 - 60 Å	Ionization Chamber	Solar X-ray Monitor
	1 - 20 Å	Ionization Chamber	Solar X-ray Monitor
6	1080 - 1350 Å	Scanning Ionization Chamber	Solar Lyman Alpha Bursts
7A	1080 - 1350 Å	2 - Ionization Chambers	Solar Lyman Alpha Monitor
7B	1080 - 1350 Å	2 - Ionization Chambers	Solar Ultra-Violet Monitor
8	1225 - 1350 Å	Ionization Chamber	Solar UV Continuum Flash
9	1500 - 1700 Å	Ionization Chamber ($5^\circ \angle$ to sunline)	Background X-ray level
10A	0.5 - 3 Å	Ionization Chamber ($5^\circ \angle$ to sunline)	Background X-ray level
10B	1 - 8 Å	Cs I (Na) Scintillating Crystal and Photomultiplier	
11	0.1 - 0.5 Å (20 - 150 keV)	Lif Photometer	Solar Hard X-ray Monitor
12	170 - 600 Å	Ionization Chamber	Solar Excitation of F-layer
13	0.1 - 1.6 Å	Thermistor	Solar Hard X-ray Continuum
14	Degrees Temperature	Large-Area Proportional Counter	Skin Anti-solar Temperature
15	0.5 - 15 Å		Stellar X-ray Variations (STELLRAD)
	Aspect Sensors		Housekeeping Sensors

Table 3
O, N₂, O₂, and NO Absorption and Ionization Cross Sections for Each Solar Line or Band

BAND	FLUX	CROSS SECTIONS (MBN)						SIGT _{O2}	SIGI _{O2}
		N	SIGT _N	SIGI _N	N ₂	SIGT _{N₂}	SIGI _{N₂}		
6.1	1.30E 08	0.0	0.0	0.0	0.400	0.0	19	17.100	7.200
6.2	2.20E 08	0.0	0.0	0.0	10.400	0.0	27	18.600	9.300
6.3	1.00E 08	0.0	0.0	0.0	0.200	0.0	19	25.300	13.900
6.4	3.90E 08	0.0	0.0	0.0	5.200	0.0	27	14.500	7.000
6.5	8.00E 08	0.0	0.0	0.0	300.000	0.0	27	21.900	10.500
6.6	4.40E 09	0.0	0.0	0.0	0.100	0.0	21	20.800	12.500
6.7	6.00E 08	0.0	0.0	0.0	0.100	0.0	2;	18.200	8.900
6.8	3.50E 09	0.0	0.0	0.0	0.0	0.0		19.300	10.000
6.9	3.00E 11	0.0	0.0	0.0	0.0	0.0		2.400	2.000
7.0	4.00E 09	0.0	0.0	0.0	0.0	0.0		13.800	8.500
7.1	1.70E 09	0.0	0.0	0.0	0.0	0.0		15.600	9.400
7.2	5.90E 08	0.0	0.0	0.0	0.0	0.0		8.600	6.500
7.3	2.20E 08	0.0	0.0	0.0	0.0	0.0		3.400	2.700
7.4	2.70E 08	0.0	0.0	0.0	0.0	0.0		3.600	3.000
7.5	2.20E 09	0.0	0.0	0.0	0.0	0.0		2.500	1.200
7.6	3.60E 09	0.0	0.0	0.0	0.0	0.0		2.100	1.800
7.7	4.30E 08	0.0	0.0	0.0	0.0	0.0		2.100	0.300
7.8	2.90E 08	0.0	0.0	0.0	0.0	0.0		2.100	0.100
7.9	2.30E 08	0.0	0.0	0.0	0.0	0.0		2.100	0.0
8.0	4.60E 08	0.0	0.0	0.0	0.0	0.0		2.000	0.0
8.1	5.40E 08	0.0	0.0	0.0	0.0	0.0		1.700	0.0
8.2	9.90E 08	0.0	0.0	0.0	0.0	0.0		1.900	0.0
8.3	2.70E 12	0.0	0.0	0.0	0.0	0.0		0.0	0.0
							Est.	2.100	0.0

Table 3 (Continued)

BAND	FLUX	CROSS SECTIONS (MBN)						SIGT	SIGI	NO	SIGT	SIGI	NO	SIGT	SIGI
		0	SIGT	SIGI	N2	SIGT	SIGI								
31	1.90E 08	15.198	4.317		24.500	23.800	Est.	21	22.000	22.000			21	21.000	17.000
32	3.10E 08	15.354	4.429		25.000	24.000	Est.	21	20.000	20.000			21	26.000	21.000
33	8.90E 08	15.348	4.515		23.100	23.100	Est.	21	23.000	22.000			26	22.300	18.900
34	8.00E 07	15.288	4.552		23.400	22.200	Est.	21	25.000	23.000			26	28.000	25.300
35	5.00E 08	15.226	4.575		23.700	23.700	Est.	21	24.000	23.000			20	28.300	24.700
36	2.50E 08	15.099	4.605		24.000	24.000	Est.	21	23.300	22.800			20	27.000	25.400
37	9.20E 08	15.055	4.612		24.000	24.000	21		21.500	21.300			26	30.000	29.200
38	3.90E 08	10.773	4.696		50.000	50.000	Est.		21.000	18.300			26	22.000	19.000
39	2.30E 08	10.855	4.693		26.000	20.000	26,27		21.600	18.100			26	31.600	15.800
40	4.00E 07	10.945	4.690		23.000	21.000	Est.		20.400	18.400			25	24.000	20.000
41	9.00E 07	10.575	4.699		23.000	21.000	Est.		25.000	18.200			25	18.000	11.000
42	8.00E 07	4.690	4.690		19.800	11.300	21		30.000	18.000			21	18.500	9.500
43	1.90E 08	4.687	4.687		37.000	21.000	Est.		23.000	14.000			21	18.000	11.000
44	1.80E 08	4.687	4.687		85.400	65.800	21		23.000	14.000			23	24.300	9.700
45	2.30E 08	4.684	4.684		15.000	8.900	21,27		16.700	10.000			23	22.100	11.000
46	1.20E 08	4.677	4.677		19.000	13.300	21,27		7.800	5.900			23	31.400	10.400
47	8.00E 07	4.671	4.671		22.300	19.800	21,27		16.400	7.400			23	28.000	10.400
48	1.30E 08	4.669	4.669		9.000	8.000	27		17.600	9.800			21	24.000	13.500
49	2.60E 08	4.666	4.666		22.000	10.000	27		17.100	9.600			21	27.700	10.200
50	3.90E 08	4.672	4.672		25.000	12.000	Est.		12.000	6.600			21	26.000	10.000
51	7.80E 08	4.635	4.635		20.000	0.0	Est.		16.000	8.500			21	18.000	7.000
52	5.20E 08	4.600	4.600		9.200	0.0			19.700	9.800			23	13.600	6.800
53	1.50E 09	4.581	4.581		5.200	0.0	Est.		25.000	11.000			21	9.000	4.500
54	1.00E 08	4.515	4.515		6.000	0.0	Est.		26.000	12.000			21	9.200	4.500
55	2.70E 09	4.512	4.512		5.000	0.0	Est.		28.000	12.500			23	7.000	3.500
56	1.30E 08	4.429	4.429		6.300	0.0	27		25.300	10.000			23	10.600	8.600
57	3.20E 09	4.441	4.441		4.000	0.0	18,27		30.000	14.000			23	9.300	4.500
58	1.20E 09	0.0	0.0		7.600	0.0	Est.		32.000	15.000			23	7.500	3.200
59	1.30E 08	0.0	0.0		7.400	0.0	27		33.500	16.700			23	6.900	5.500
60	1.30E 08	0.0	0.0		4.800	0.0	27		32.000	9.600			23	26.000	17.000

Table 3 (Continued)

BAND	FLUX	CROSS SECTIONS (MBN)						SIGT	SIGI	SIGT	SIGI
		0	SIGT	SIGI	N2	SIGT	SIGI				
1	1.00E-01	0.000	0.034	0.000	0.038	0.000	0.054	0.000	0.069	0.004	0.550
2	3.00E 01	0.002	0.270	0.002	0.320	0.003	0.435	0.015	1.140	0.019	1.444
3	2.50E 03	0.009	0.720	0.011	0.836	0.029	1.566	0.039	2.133	0.050	2.700
4	2.80E 04	0.025	1.300	0.029	1.520	0.060	2.520	0.080	3.310	0.100	4.100
5	1.80E 05	0.050	2.100	0.086	0.950	0.118	1.325	0.150	1.700	0.290	2.400
6	4.00E 06	0.080	0.890	0.170	1.400	0.230	1.900	0.410	2.750	0.520	3.500
7	5.30E 07	0.166	1.300	0.300	2.000	0.230	1.600	0.315	2.250	0.400	2.900
8	8.30E 07	0.250	1.700	0.480	2.600	0.480	2.600	0.645	3.500	0.810	4.400
9	2.40E 07	0.230	1.700	0.670	3.100	0.670	3.100	0.885	4.700	1.100	6.300
10	1.10E 08	0.390	2.100	1.000	2.900	0.890	3.600	1.195	5.700	1.500	7.800
11	1.00E 08	0.550	2.600	1.700	3.600	1.200	4.300	1.600	6.850	2.000	9.400
12	1.30E 08	0.750	3.700	2.700	5.100	2.700	5.400	2.850	6.450	3.000	7.500
13	1.20E 08	1.000	5.100	4.000	6.000	4.400	9.000	4.000	11.000	5.200	10.000
14	4.00E 08	1.700	6.000	5.000	7.000	5.600	11.000	5.600	13.000	6.400	13.000
15	9.00E 08	3.000	8.000	6.000	11.000	7.000	14.000	12.000	24.000	10.000	20.000
16	3.70E 09	4.000	8.000	4.000	11.000	8.000	16.000	12.000	24.000	15.000	22.000
17	1.40E 09	6.500	13.000	6.500	14.000	10.000	13.000	18.000	36.000	15.000	39.000
18	3.10E 09	7.500	15.000	11.200	23.000	13.000	26.000	16.000	32.000	13.000	26.000
19	2.40E 09	11.200	3.300	10.102	3.025	8.000	16.000	16.18	18.000	13.000	16.
20	1.10E 09	10.9	10.102	3.180	12.100	24.200	16.18	14.000	28.000	16.600	33.200
21	5.40E 09	10.752	3.180	11.95	3.411	10.000	10.000	16.18	15.000	18.000	36.000
22	7.20E 08	11.695	3.411	12.415	3.580	12.000	12.000	16.18	19.000	17.000	17.000
23	3.60E 08	12.415	3.580	12.529	3.607	12.000	12.000	16.18	19.000	17.000	17.000
24	1.70E 08	12.529	3.607	12.612	3.627	12.000	12.000	16.18	19.000	17.000	17.000
25	5.60E 08	12.612	3.627	13.771	3.910	15.000	14.700	Est.,18	17.000	20.000	20.000
26	6.30E 08	13.771	3.910	15.328	4.401	23.000	23.000	Est.	18.000	23.000	23.000
27	4.40E 08	15.328	4.401	14.572	4.084	24.000	24.000	Est.	22.000	22.000	22.000
28	6.60E 08	15.006	4.233	24.200	24.200	24.000	24.000	Est.	22.000	22.000	22.000
29	3.80E 08	15.091	4.267	24.000	24.000	24.000	24.000	Est.,21	22.000	22.000	22.000
30	8.00E 07	15.091	4.267	24.000	24.000	24.000	24.000	Est.	22.000	22.000	22.000

Table 4
Total Ion Production Rates from O, O₂, and N₂ for 1-1215Å as a Function of Altitude

TOTAL (183 LINES) ION PRODUCTION RATE

Z	O	N ₂	O ₂	SUM
6.00E 01	2.08E-14	1.23E-05	5.51E-06	1.78E-05
7.00E 01	4.61E-11	7.48E-04	3.21E-04	1.07E-03
8.00E 01	1.38E-05	5.62E-02	2.60E-02	8.23E-02
9.00E 01	2.13E-02	9.31E 00	4.91E 00	1.42E 01
1.00E 02	1.72E 01	3.19E 02	1.36E 03	1.70E 03
1.10E 02	6.87E 01	6.57E 02	2.29E 03	3.02E 03
1.20E 02	2.23E 02	1.04E 03	1.24E 03	2.50E 03
1.30E 02	6.02E 02	2.05E 03	9.31E 02	3.58E 03
1.40E 02	8.82E 02	2.71E 03	8.63E 02	4.45E 03
1.50E 02	1.03E 03	2.87E 03	7.59E 02	4.66E 03
1.60E 02	1.08E 03	2.70E 03	6.31E 02	4.41E 03
1.70E 02	1.07E 03	2.41E 03	5.09E 02	3.98E 03
1.80E 02	1.02E 03	2.06E 03	4.02E 02	3.48E 03
1.90E 02	9.46E 02	1.72E 03	3.12E 02	2.98E 03
2.00E 02	8.65E 02	1.41E 03	2.40E 02	2.51E 03
2.10E 02	7.80E 02	1.14E 03	1.83E 02	2.10E 03
2.20E 02	6.96E 02	9.09E 02	1.39E 02	1.74E 03
2.30E 02	6.18E 02	7.22E 02	1.05E 02	1.44E 03
2.40E 02	5.45E 02	5.70E 02	7.92E 01	1.19E 03
2.50E 02	4.79E 02	4.48E 02	5.96E 01	9.86E 02
2.60E 02	4.19E 02	3.51E 02	4.48E 01	8.14E 02
2.70E 02	3.66E 02	2.74E 02	3.36E 01	6.73E 02
2.80E 02	3.19E 02	2.13E 02	2.52E 01	5.57E 02
2.90E 02	2.77E 02	1.66E 02	1.89E 01	4.62E 02
3.00E 02	2.41E 02	1.29E 02	1.41E 01	3.84E 02
3.10E 02	2.09E 02	1.00E 02	1.06E 01	3.20E 02
3.20E 02	1.81E 02	7.78E 01	7.91E 00	2.67E 02
3.30E 02	1.57E 02	6.04E 01	5.92E 00	2.23E 02
3.40E 02	1.36E 02	4.69E 01	4.42E 00	1.87E 02
3.50E 02	1.18E 02	3.64E 01	3.31E 00	1.58E 02
3.60E 02	1.02E 02	2.82E 01	2.47E 00	1.33E 02
3.70E 02	8.85E 01	2.19E 01	1.85E 00	1.12E 02
3.80E 02	7.67E 01	1.70E 01	1.39E 00	9.51E 01
3.90E 02	6.65E 01	1.32E 01	1.04E 00	8.07E 01
4.00E 02	5.76E 01	1.03E 01	7.79E-01	6.87E 01
4.10E 02	4.99E 01	8.00E 00	5.84E-01	5.85E 01
4.20E 02	4.33E 01	6.22E 00	4.38E-01	4.99E 01
4.30E 02	3.75E 01	4.85E 00	3.29E-01	4.27E 01
4.40E 02	3.25E 01	3.77E 00	2.47E-01	3.66E 01
4.50E 02	2.82E 01	2.94E 00	1.86E-01	3.14E 01
4.60E 02	2.45E 01	2.29E 00	1.40E-01	2.69E 01
4.70E 02	2.13E 01	1.79E 00	1.05E-01	2.32E 01
4.80E 02	1.85E 01	1.40E 00	7.94E-02	1.99E 01
4.90E 02	1.60E 01	1.09E 00	5.99E-02	1.72E 01
5.00E 02	1.39E 01	8.54E-01	4.52E-02	1.48E 01
5.10E 02	1.21E 01	6.68E-01	3.41E-02	1.28E 01
5.20E 02	1.05E 01	5.23E-01	2.58E-02	1.11E 01
5.30E 02	9.16E 00	4.10E-01	1.95E-02	9.59E 00
5.40E 02	7.97E 00	3.21E-01	1.48E-02	8.31E 00
5.50E 02	6.94E 00	2.52E-01	1.12E-02	7.21E 00
5.60E 02	6.05E 00	1.98E-01	8.50E-03	6.25E 00

Table 5
The New Bands and Their Wavelength Intervals

Band	Wavelength (Å)	Lines and Bands
1	0-2	1
2	2-4	2
3	4-6	3
4	6-8	4
5	8-10	5
6	33.6	6
7	40-50	7
8	50-60	8
9	60-80	9-11
10	80-100	12,13
11	100-205	14-16
12	205-370	17-20
13	303-368	21-25
14	370-730	26-37
15	630-800	38-50
16	800-911	51-54
17	860-911	55-57
18	911-972	58-65
19	977-990	66-68
20	1025	69-82
21	1215-1304	83
22	Others	

ALI AND KEPPEL

Table 6
The Fluxes and Cross Sections Appropriate to the Bands of Table 6

BAND	FLUX	CROSS SECTIONS (WMN)						NO. 02					
		SIG1	SIG1	SIG1	SIG1	SIG1	SIG1	SIG1	SIG1	SIG1	SIG1	SIG1	SIG1
1	1.00F-01	0.000	0.034	0.000	0.038	0.000	0.054	0.000	0.054	0.000	0.060	0.000	0.060
2	3.00E-01	0.002	0.270	0.002	0.320	0.003	0.435	0.004	0.550	0.004	0.550	0.004	0.550
3	2.50E-03	0.009	0.720	0.011	0.836	0.015	1.140	0.019	1.444	0.019	1.444	0.019	1.444
4	2.80E-04	0.025	1.300	0.029	1.564	0.039	2.133	0.050	2.700	0.050	2.700	0.050	2.700
5	1.80E-05	0.050	2.100	0.060	2.520	0.080	3.310	0.100	4.100	0.100	4.100	0.100	4.100
6	4.00E-06	0.080	0.890	0.086	0.950	0.118	1.325	0.150	1.700	0.150	1.700	0.150	1.700
7	4.70E-07	0.160	1.300	0.170	1.400	0.230	1.900	0.290	2.400	0.290	2.400	0.290	2.400
8	8.30E-07	0.250	1.700	0.300	2.000	0.410	2.750	0.520	3.500	0.520	3.500	0.520	3.500
9	1.04E-08	0.468	2.342	0.572	2.842	0.761	4.081	0.951	5.321	0.951	5.321	0.951	5.321
10	2.20E-08	0.864	3.264	1.031	3.918	1.379	6.223	1.727	8.527	1.727	8.527	1.727	8.527
11	5.00E-09	3.636	7.408	5.152	10.192	12.168	24.396	5.912	12.020	5.912	12.020	5.912	12.020
12	7.63E-09	8.693	9.794	9.059	17.075	16.367	32.734	13.794	24.338	13.794	24.338	13.794	24.338
13	7.21E-09	11.116	3.268	11.875	20.938	14.856	29.711	16.800	31.031	16.800	31.031	16.800	31.031
14	5.33E-09	14.956	4.372	22.756	22.620	21.337	22.997	24.483	21.950	24.483	21.950	24.483	21.950
15	2.41E-09	6.578	4.683	31.788	23.699	18.522	12.547	24.587	12.592	24.587	12.592	24.587	12.592
16	2.90E-09	4.597	4.597	6.926	0.0	21.663	10.147	12.246	5.585	12.246	5.585	12.246	5.585
17	6.03E-09	4.473	4.473	4.497	0.0	29.093	13.242	8.298	4.141	8.298	4.141	8.298	4.141
18	3.10E-09	0.0	0.0	82.288	0.0	25.463	11.910	14.547	10.660	14.547	10.660	14.547	10.660
19	5.00E-09	0.0	0.0	0.100	0.0	20.488	12.068	3.697	2.308	3.697	2.308	3.697	2.308
20	3.50E-09	0.0	0.0	0.0	0.0	19.300	10.000	1.520	0.980	1.520	0.980	1.520	0.980
21	3.00E-09	0.0	0.0	0.0	0.0	2.400	2.000	0.010	0.0	0.010	0.0	0.010	0.0
22	1.75E-10	0.0	0.0	0.0	0.0	7.699	4.652	3.914	0.0	3.914	0.0	3.914	0.0
23	2.70E-12	0.0	0.0	0.0	0.0	0.0	0.0	2.100	0.0	2.100	0.0	2.100	0.0

Table 7
The Total Ion Production Rate Profiles of the Contracted Bands of Table 6

TOTAL (23 BANDS) ION PRODUCTION RATE

T	O	N2	O2	SUM
6.00E 01	2.08E-14	1.23E-05	5.51E-06	1.78E-05
7.00E 01	4.61E-11	7.43E-04	3.21E-04	1.07E-03
8.00E 01	1.38E-05	5.62E-02	2.60E-02	8.23E-02
9.00E 01	2.13E-02	9.31E 00	4.90E 00	1.42E 01
1.00E 02	1.67E 01	3.08E 02	1.30E 03	1.62E 03
1.10E 02	6.63E 01	6.34E 02	2.29E 03	2.99E 03
1.20E 02	1.97E 02	9.62E 02	1.16E 03	2.32E 03
1.30E 02	5.56E 02	2.01E 03	8.43E 02	3.41E 03
1.40E 02	8.43E 02	2.72E 03	8.02E 02	4.36E 03
1.50E 02	1.00E 03	2.91E 03	7.21E 02	4.63E 03
1.60E 02	1.06E 03	2.75E 03	6.07E 02	4.42E 03
1.70E 02	1.06E 03	2.46E 03	4.95E 02	4.02E 03
1.80E 02	1.01E 03	2.11E 03	3.94E 02	3.52E 03
1.90E 02	9.43E 02	1.76E 03	3.09E 02	3.01E 03
2.00E 02	8.63E 02	1.44E 03	2.39E 02	2.54E 03
2.10E 02	7.79E 02	1.16E 03	1.83E 02	2.12E 03
2.20E 02	6.96E 02	9.23E 02	1.40E 02	1.76E 03
2.30E 02	6.18E 02	7.31E 02	1.06E 02	1.46E 03
2.40E 02	5.45E 02	5.76E 02	8.01E 01	1.20E 03
2.50E 02	4.79E 02	4.51E 02	6.03E 01	9.90E 02
2.60E 02	4.19E 02	3.53E 02	4.53E 01	8.17E 02
2.70E 02	3.66E 02	2.75E 02	3.39E 01	6.75E 02
2.80E 02	3.19E 02	2.14E 02	2.54E 01	5.58E 02
2.90E 02	2.77E 02	1.67E 02	1.90E 01	4.63E 02
3.00E 02	2.41E 02	1.29E 02	1.42E 01	3.84E 02
3.10E 02	2.09E 02	1.00E 02	1.06E 01	3.20E 02
3.20E 02	1.81E 02	7.80E 01	7.94E 00	2.67E 02
3.30E 02	1.57E 02	6.05E 01	5.93E 00	2.24E 02
3.40E 02	1.36E 02	4.69E 01	4.43E 00	1.88E 02
3.50E 02	1.18E 02	3.64E 01	3.31E 00	1.58E 02
3.60E 02	1.02E 02	2.83E 01	2.48E 00	1.33E 02
3.70E 02	8.85E 01	2.19E 01	1.85E 00	1.12E 02
3.80E 02	7.67E 01	1.70E 01	1.39E 00	9.51E 01
3.90E 02	6.65E 01	1.32E 01	1.04E 00	8.07E 01
4.00E 02	5.76E 01	1.03E 01	7.79E-01	6.87E 01
4.10E 02	4.99E 01	8.00E 00	5.84E-01	5.85E 01
4.20E 02	4.33E 01	6.23E 00	4.38E-01	4.99E 01
4.30E 02	3.75E 01	4.85E 00	3.29E-01	4.27E 01
4.40E 02	3.25E 01	3.78E 00	2.47E-01	3.66E 01
4.50E 02	2.82E 01	2.94E 00	1.86E-01	3.14E 01
4.60E 02	2.45E 01	2.29E 00	1.40E-01	2.69E 01
4.70E 02	2.13E 01	1.79E 00	1.05E-01	2.32E 01
4.80E 02	1.85E 01	1.40E 00	7.94E-02	1.99E 01
4.90E 02	1.60E 01	1.09E 00	5.99E-02	1.72E 01
5.00E 02	1.39E 01	8.54E-01	4.52E-02	1.48E 01
5.10E 02	1.21E 01	6.68E-01	3.41E-02	1.28E 01
5.20E 02	1.05E 01	5.23E-01	2.58E-02	1.11E 01
5.30E 02	9.16E 00	4.10E-01	1.95E-02	9.59E 00
5.40E 02	7.97E 00	3.21E-01	1.48E-02	8.31E 00
5.50E 02	6.94E 00	2.52E-01	1.12E-02	7.21E 00
5.60E 02	6.05E 00	1.98E-01	8.50E-03	6.25E 00

Table 8
Densities of Some Atmospheric Species as a Function of Altitude

ALT.	O	N2	NO	O2
80.	8.50E 10	2.96E 14	2.21E 08	7.95E 13
90.	1.25E 11	4.96E 13	1.50E 08	1.33E 13
100.	5.00E 11	8.18E 12	1.06E 08	1.99E 12
110.	2.00E 11	1.62E 12	7.78E 07	3.49E 11
120.	7.60E 10	4.00E 11	5.85E 07	7.50E 10
130.	3.28E 10	1.25E 11	4.50E 07	2.11E 10
140.	1.92E 10	5.81E 10	3.53E 07	9.13E 09
150.	1.29E 10	3.24E 10	2.81E 07	4.79E 09
160.	9.43E 09	2.00E 10	2.28E 07	2.80E 09
170.	7.21E 09	1.32E 10	1.87E 07	1.76E 09
180.	5.69E 09	9.04E 09	1.55E 07	1.15E 09
190.	4.60E 09	6.40E 09	1.30E 07	7.81E 08
200.	3.78E 09	4.62E 09	1.09E 07	5.41E 08
210.	3.14E 09	3.39E 09	9.33E 06	3.81E 08
220.	2.63E 09	2.52E 09	8.01E 06	2.72E 08
230.	2.22E 09	1.89E 09	6.92E 06	1.96E 08
240.	1.88E 09	1.42E 09	6.02E 06	1.42E 08
250.	1.60E 09	1.08E 09	5.26E 06	1.04E 08
260.	1.37E 09	8.23E 08	4.63E 06	7.61E 07
270.	1.17E 09	6.29E 08	4.09E 06	5.60E 07
280.	1.00E 09	4.83E 08	3.63E 06	4.14E 07
290.	8.63E 08	3.71E 08	3.24E 06	3.06E 07
300.	7.43E 08	2.85E 08	2.89E 06	2.27E 07
310.	6.40E 08	2.20E 08	2.60E 06	1.69E 07
320.	5.52E 08	1.70E 08	2.34E 06	1.26E 07
330.	4.76E 08	1.32E 08	2.12E 06	9.38E 06
340.	4.11E 08	1.02E 08	1.92E 06	7.01E 06
350.	3.56E 08	7.90E 07	1.75E 06	5.24E 06
360.	3.08E 08	6.13E 07	1.59E 06	3.92E 06
370.	2.66E 08	4.76E 07	1.46E 06	2.94E 06
380.	2.31E 08	3.70E 07	1.33E 06	2.20E 06
390.	2.00E 08	2.88E 07	1.22E 06	1.66E 06
400.	1.73E 08	2.24E 07	1.13E 06	1.24E 06
410.	1.50E 08	1.75E 07	1.04E 06	9.36E 05
420.	1.30E 08	1.36E 07	9.60E 05	7.05E 05
430.	1.13E 08	1.07E 07	8.89E 05	5.31E 05
440.	9.82E 07	8.33E 06	8.24E 05	4.00E 05
450.	8.54E 07	6.51E 06	7.66E 05	3.02E 05
460.	7.42E 07	5.09E 06	7.12E 05	2.28E 05
470.	6.45E 07	3.99E 06	6.64E 05	1.73E 05
480.	5.61E 07	3.13E 06	6.20E 05	1.31E 05
490.	4.89E 07	2.45E 06	5.79E 05	9.90E 04
500.	4.25E 07	1.92E 06	5.42E 05	7.51E 04
510.	3.70E 07	1.51E 06	5.08E 05	5.70E 04
520.	3.23E 07	1.19E 06	4.77E 05	4.32E 04
530.	2.81E 07	9.34E 05	4.48E 05	3.29E 04
540.	2.45E 07	7.35E 05	4.21E 05	2.50E 04
550.	2.14E 07	5.79E 05	3.96E 05	1.90E 04
560.	1.87E 07	4.56E 05	3.74E 05	1.45E 04
570.	1.63E 07	3.60E 05	3.53E 05	1.10E 04
580.	1.43E 07	2.84E 05	3.33E 05	8.43E 03